

Contents lists available at [ScienceDirect](https://www.sciencedirect.com)

International Journal of Mechanical Sciences

journal homepage: www.elsevier.com/locate/ijmecsci

Lattice Boltzmann method for particulate multiphase flow system

Qiangqiang Li, Guang Yang, Yunfan Huang, Xukang Lu, Jingchun Min, Moran Wang*

Department of Engineering Mechanics, Tsinghua University, Beijing 100084, China

ARTICLE INFO

Keywords:

Complex fluids
Lattice Boltzmann
Two-fluid model
Gel particle suspension
Multiphase flow

ABSTRACT

This study proposes a numerical model for particulate three-phase flow in microchannels based on multiphase lattice Boltzmann method (LBM). The model combines the color-gradient method to track the immiscible fluid-fluid interface and the two-fluid model (TFM) to describe particle-particle and particle-fluid interactions, which can efficiently simulate transport and displacement processes involving large amounts of particles. A mixture-rheology TFM algorithm is proposed by introducing a mixture phase with rheology properties obtained from experiments instead of the conventional TFM particle phase with artificial viscosity models. Multi-relaxation-time (MRT) collision operator and GPU computing are adopted to enhance the numerical stability and efficiency. Various theoretical benchmarks for particle transport and two-phase flow are performed respectively to verify the accuracy of the proposed model. Exceptional consistency between results from particulate three-phase flow simulation and microfluidic experiments further confirms the reliability of our model, especially in capturing the inertial lagging and accumulation phenomena under multiphase and porous flow conditions. The proposed numerical framework will benefit our understanding of multiphase displacement with microgels in microchannels with complex geometries.

1. Introduction

Particulate three phase flow in porous media is commonly encountered in natural and industrial applications, such as energy resource recovery, wastewater treatment and monitoring of pollutant transport underground [1–4]. For example, microgel particles have been developed as effective additives with huge benefits for oil production around the world. Displacement of oil by microgel particle suspensions is a typical water-oil-particle three-phase flow process in rocks [5,6], wherein the microgel suspension is composed of water and dispersed microgel particles. Due to the complex cross-linked network structures of polymer molecules, the fluid-particle and particle-particle interactions at the microscale is hard to be characterized, which manifest as complex non-Newtonian rheology characteristics of the suspension at the macroscale [7–9]. In addition, the inertial effect cannot be ignored for micron-sized particles, which may pose significant impacts on particle distribution and thereby multiphase interfacial movement. However, the fundamental physical mechanisms of such three-phase flow in microchannels remain unclarified. To simulate the multiphase transport process in pores of water-oil-particle system, an accurate and efficient numerical model combining interface evolution and particle migration is urgently needed.

Quite a few numerical methods have been developed for gel particle flooding at the pore scale [10–13] to reveal the fundamental mechanisms, facilitated with the advantages of depicting the particles migration and interface evolution processes in details [10,14]. The models tracking particle flows can be divided into two categories: Eulerian-Lagrangian and Eulerian-Eulerian methods [15]. In the Eulerian-Lagrangian method, the fluid phase, i.e. continuous phase, is tracked by the Eulerian method and solved by the Navier-Stokes equation, while the particle phase, i.e. the discrete phase, is tracked by the Lagrangian method and solved by Newton's second law [16–18]. Immersed boundary method (IBM) is a popular fluid-structure interaction method, which has been applied into studying the deformation and migration of microgel particles in pores [19–21], where the interactions between particles, fluid and walls are fully resolved by integrating along the solid-fluid interfaces. Therefore, it requires that the grid size is much smaller than single particle size and no other fluid-solid interaction models are included. As a result, IBM is the most accurate but too expensive to simulate a large amount of particles [22]. To improve the computational efficiency, discrete element method (DEM) has been developed and applied to study the particles retention and aggregation mechanisms in microchannels and porous media [23–25]. Drag and collision models should be introduced to describe the fluid-particle and

* Corresponding author.

E-mail address: mrwang@tsinghua.edu.cn (M. Wang).<https://doi.org/10.1016/j.ijmecsci.2024.109217>

Received 22 August 2023; Received in revised form 21 March 2024; Accepted 22 March 2024

Available online 24 March 2024

0020-7403/© 2024 Elsevier Ltd. All rights reserved.

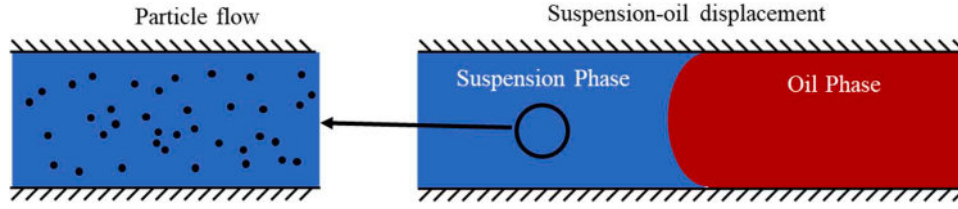


Fig. 1. Illustration of the three-phase system. For convenience, we take water-oil-particle system as an example hereafter. The blue part represents the suspension phase, the red part represents the oil phase, and the black dots represent suspended particles.

particle-particle interactions to achieve better efficiency [26]. However, it should be stressed that the particle number and applicable system scale are still limited in those simulations since each particle need to be tracked and the interaction between particles need to be solved.

Eulerian-Eulerian method increases the computational efficiency greatly by treating both fluid and particles phase as continuum and using Eulerian method to track both phases. Lei et al. applied advection-diffusion equation (ADE) to simulate the transport of microgel particles in porous media which neglects the volume fraction of particles and realizes the high-performance simulation of microgel particle flooding process in a complex porous model [27]. However, ADE is unable to describe the inertial effects of large gel particles and the complex interactions at a high concentration, which brings in deviations from experiments. Therefore, how to develop an efficient and accurate numerical method for gel suspensions transport remains an open question.

The two-fluid model is a classical Eulerian-Eulerian method, in which the particle phase is treated as another fluid and solved via the Navier-Stokes equation [28]. In this method, the fluid-particle and particle-particle interactions are described by drag and other interaction models [29]. It has a prominent advantage of high efficiency because it focuses on the movement of particle groups rather than individual particles, and has the potential to take account of particle inertial effects by considering the momentum conservation of particles [26]. As a result, this approach is frequently employed in simulations of fluidized bed [29], blood cells flow [30,31] and other particulate multiphase flows that involves large numbers of particles or bubbles [32] and promising to study the collective transport of microgel particles in porous media.

Besides the particle-in-water suspension phase, the fluid-fluid interface between suspension and oil also requires to be resolved in the water-oil-particle three phase system. In literatures, level-set and volume-of-fluid (VOF) as traditional multiphase models have been applied to capture the fluid-fluid interface under the framework of finite-element and finite-volume methods, which can be coupled with direct-simulation particle model to solve fluid-particle interaction [33–35]. However, the algorithm of traditional interface capturing is complicated especially with handling phases interactions, and hard to handle the complex boundary conditions efficiently in porous structure [36]. On the other hand, multiphase lattice Boltzmann method has been developed for twenty years with its advantages of handling complex boundaries efficiently and easy implementation on modern parallel computers [37–40], which is quite suitable for transport problems in porous media. Many multiphase LBM models have been proposed such as color-gradient model [41], pseudo-potential model [42,43], free-energy model [44], among which the color-gradient model introduces ‘red’ and ‘blue’ particle distribution function to represent two immiscible fluids and uses recolor operator to achieve fluids separation [45]. The color-gradient LBM is able to adjust fluid properties separately such as viscosity, surface tension and contact angle, and has been developed for simulating large-viscosity-ratio systems [46]. Therefore, it is widely used to simulate multiphase flows in porous media, especially for complex fluid systems like the microgel particle suspension [47,48].

In this paper, we aim to develop a new simulation framework to

capture the coupling transport process involving both interface evolution and microgel particle migration. Our model combines the color-gradient model with a modified two-fluid model (Section 2), both of which are solved by MRT-LBM based on GPU computing. This method offers several advantages, including high-performance interface and particle tracking, as well as the ability to handle complex rheology of microgel particle suspensions. The numerical method is then validated by comparisons with theoretical and experimental results (Section 3). The results demonstrate that the proposed method can accurately capture particle inertial lagging and accumulation phenomena observed in experiments. This method provides an accurate and efficient approach to simulate microgel transport as well as multiphase flow in microchannels, which will help elucidate underlying pore-scale transport mechanisms.

2. Methods

In this section, the numerical method is introduced including governing equations, lattice Boltzmann method for suspension-oil displacement and particulate flow, and multiple relaxation time scheme for non-Newtonian fluid. Modification on the traditional two-fluid model and combination with color-gradient method serve for the accurate and efficient simulation of particulate multiphase flow systems.

2.1. Governing equations

To streamline our description, we take the water-oil-particle system as an example in the following text. As Fig. 1 shows, the macroscopic physical process consists of two immiscible fluids, i.e., the suspension phase (water + particles), and the oil phase.

The governing equations for the displacing phase (suspension) and the displaced phase (oil) can be represented by a set of mass and momentum equations as

$$\frac{\partial \rho}{\partial t} + \nabla \cdot (\rho \mathbf{u}) = 0, \quad (1)$$

$$\frac{\partial (\rho \mathbf{u})}{\partial t} + \nabla \cdot (\rho \mathbf{u} \mathbf{u}) = -\nabla p + \nabla \cdot \boldsymbol{\tau} + \mathbf{F}_s + \mathbf{F}_{\text{ext}}, \quad (2)$$

$$\boldsymbol{\tau} = \mu (\nabla \mathbf{u} + (\nabla \mathbf{u})^T), \quad (3)$$

where the ρ , \mathbf{u} , p , $\boldsymbol{\tau}$ denote the density, the velocity vector, the pressure and the shear stress tensor, respectively. \mathbf{F}_s and \mathbf{F}_{ext} indicate the body force accounting for surface tension and the other external forces, and μ is the dynamic viscosity.

The displacing phase is the suspension consisting of water and microgel particles. The volume fraction of microgel particles is generally lower than 10%, but the number of microgel particles is huge and thus the overall behavior of particles is model by a fluid model. Therefore, the suspension can be modeled by a two-fluid model. In the classical two-fluid models, both the fluid phase and the particle phase are described by their own N-S equations respectively, while the particle-particle interaction is described by the viscosity term of the particle phase. A few models have been proposed to determine the viscosity of the particle

phase [7,30,49–51]. However, it is difficult to characterize the viscosity of the discrete phase (microgel particles) as a fluid quantitatively. Therefore, we focus on the suspension phase whose viscosity can be obtained directly from experiments, instead of the microgel particle phase. Meanwhile, the volume fraction and the velocity of particles can be calculated based on the local mass and momentum conservation. Since the suspension phase has been involved in the suspension-oil displacement process i.e., described by Eqs. (1) and (2), only the N-S equations for the fluid phase are required, which are expressed as

$$\frac{\partial(\alpha_f \rho)}{\partial t} + \nabla \cdot (\alpha_f \rho \mathbf{u}_f) = 0. \quad (4)$$

$$\frac{\partial(\alpha_f \rho \mathbf{u}_f)}{\partial t} + \nabla \cdot (\alpha_f \rho \mathbf{u}_f \mathbf{u}_f) = -\alpha_f \nabla p + \nabla \cdot (\alpha_f \boldsymbol{\tau}_f) - \beta_d (\mathbf{u}_f - \mathbf{u}_p) + \mathbf{F}_f. \quad (5)$$

where the subscript f and p indicate the fluid and particle phase, and α , ρ , \mathbf{u} denote the volume fraction, intrinsic density and velocity vector, respectively. p , $\boldsymbol{\tau}$ and \mathbf{F} are the hydrodynamic pressure, shear tensor and external forces. The volume fraction and velocity of particle phase can be calculated indirectly by local mass and momentum conservation as

$$\alpha_p + \alpha_f = 1 \quad (6)$$

$$\rho \mathbf{u} = \rho \alpha_f \mathbf{u}_f + \rho \alpha_p \mathbf{u}_p \quad (7)$$

The third term on the right side of Eq. (5) is the drag force representing the internal interaction between fluid and particles, induced by the velocity difference of two phases, where β_d is the drag coefficient described by the Wen-Yu model as [52]

$$\left\{ \begin{array}{l} \beta_d = \frac{3}{4} C_d \frac{\rho_f \alpha_f \alpha_p |\mathbf{u}_f - \mathbf{u}_p|}{D} \alpha_f^{-2.65} \\ C_d = \begin{cases} 24/\text{Re}(1 + 0.15\text{Re}^{0.687}) & \text{Re} < 1000 \\ 0.44 & \text{Re} \geq 1000 \end{cases} \\ \text{Re} = \frac{\rho_f \alpha_f D |\mathbf{u}_f - \mathbf{u}_p|}{\mu_f} \end{array} \right. \quad (8)$$

where D is the particle diameter.

Compared with the classical two-fluid models describing the transport of the fluid phase and the particle phase, the two-fluid model in the present work focuses on the mixture phase and the fluid phase. This provides several advantages including direct application of the apparent suspension viscosity measured from experiments without artificial models, easy coupling with the color-gradient LBM model, and better numerical stability by avoiding significant viscosity differences.

2.2. Lattice Boltzmann method for suspension-oil displacement

For the suspension-oil displacement process, the color-gradient LBM is applied to capture the fluid-fluid interface, where the discrete particle distribution functions (PDF) $f_{r,i}$ and $f_{b,i}$ are employed to represent two immiscible fluids and $f_i = f_{r,i} + f_{b,i}$ is the total particle distribution function [53]. The color-gradient LBM evolution equation with the Bhatnagar–Gross–Krook (BGK) collision operator can be written as

$$f_{k,i}(\mathbf{x} + \mathbf{e}_i \Delta t, t + \Delta t) = \Omega_k^3 \left(f_{k,i}(\mathbf{x}, t) - \frac{\Delta t}{\tau_k} [f_{k,i}(\mathbf{x}, t) - f_{k,i}^{\text{eq}}(\mathbf{x}, t)] + \Delta t \cdot \mathbf{F}_{k,i} \right), \quad (9)$$

where the subscript k (or b) and r indicate the displacing and displaced phase, respectively. Ω^3 is the recolor operator to redistribute PDFs which achieves fluid separation. The relationship between macroscopic variables and PDF with a force scheme can be expressed as [54,55]

$$\rho_b = \sum_i f_{b,i}, \rho_r = \sum_i f_{r,i}, \quad (10)$$

$$\rho_b \mathbf{u}_b = \sum_i f_{b,i} \mathbf{e}_i + \frac{\Delta t}{2} \mathbf{F}_b, \rho_r \mathbf{u}_r = \sum_i f_{r,i} \mathbf{e}_i + \frac{\Delta t}{2} \mathbf{F}_r, \quad (11)$$

$$\rho = \rho_b + \rho_r, \rho \mathbf{u} = \rho_b \mathbf{u}_b + \rho_r \mathbf{u}_r, \quad (12)$$

where \mathbf{e}_i indicates the discrete velocity along the i th direction [56,57].

As a key factor in two-phase flows, the surface tension is achieved by the continuum-surface-force (CSF) model in the present work [58], which is expressed as

$$\mathbf{F}_s = \frac{1}{2} \sigma \boldsymbol{\kappa} \nabla \rho^N, \quad (13)$$

where σ is the surface tension, $\boldsymbol{\kappa}$ and ρ^N are the interface curvature and the color function, respectively, which are defined as

$$\boldsymbol{\kappa} = -[(\mathbf{I} - \mathbf{n} \otimes \mathbf{n}) \cdot \nabla] \cdot \mathbf{n}, \quad (14)$$

$$\rho^N = \frac{\rho_r - \rho_b}{\rho_r + \rho_b}, \quad (15)$$

where $\mathbf{n} = -\nabla \rho^N / |\nabla \rho^N|$ is the normal vector of interface, which needs to be corrected based on the contact angle at solid boundaries [46,59].

After collision steps, the recolor operator Ω^3 needs to be introduced to reallocate the particle distribution function and to achieve the separation of two phase, as follows [60]

$$f_{r,i}^{**} = \frac{\rho_r}{\rho_r + \rho_b} f_i^* + \beta \frac{\rho_r \rho_b}{\rho_r + \rho_b} \omega_i \frac{\nabla \rho^N}{|\nabla \rho^N|} \mathbf{e}_i, \quad (16)$$

$$f_{b,i}^{**} = \frac{\rho_b}{\rho_r + \rho_b} f_i^* - \beta \frac{\rho_r \rho_b}{\rho_r + \rho_b} \omega_i \frac{\nabla \rho^N}{|\nabla \rho^N|} \mathbf{e}_i, \quad (17)$$

f_i^* and f_i^{**} are the post-collision and the post-recolor PDF respectively, and β is a free parameter controlling the interface thickness.

2.3. Lattice Boltzmann method for particulate flow

In the proposed model, the particle distribution and movement are determined by subtracting the water phase from the suspension phase based on the local mass and momentum conservation. The displacement process involving the suspension phase has been solved by the color-gradient LBM, whereas the water phase needs to be solved additionally. The LBM scheme for water phase is similar to the color-gradient model presented above (Eq. (9)) but without the recolor step, which can be expressed as

$$g_i(\mathbf{x} + \mathbf{c}_i \Delta t, t + \Delta t) = g_i(\mathbf{x}, t) - \frac{\Delta t}{\tau_f} [g_i(\mathbf{x}, t) - g_i^{\text{eq}}(\mathbf{x}, t)] + \Delta t \cdot \widehat{F}_{f,i}, \quad (18)$$

where subscript f indicates the fluid phase and $\widehat{F}_{f,i}$ is the source term from the body force with the superscript indicating discrete velocity space. Guo's forcing scheme is adopted in this work [54], which can be written as

$$\widehat{F}_{f,i} = \left(1 - \frac{\Delta t}{2\tau_f} \right) w_i \left(\frac{3(\mathbf{e}_i \cdot \mathbf{u})}{c^2} + \frac{9(\mathbf{e}_i \cdot \mathbf{u}) \mathbf{e}_i}{c^4} \right) \cdot \mathbf{F}_f, \quad (19)$$

where c is the lattice velocity. It should be noted that the body force in two-fluid model includes two key terms

$$\mathbf{F}_f = p \nabla (\alpha_f) - \beta_d (\mathbf{u}_f - \mathbf{u}_p), \quad (20)$$

where the first term is the correction for pressure gradient in the two-fluid model considering volume average [50], and the second term is the drag force characterizing the two-phase interaction induced by velocity differences. The macroscopic variables for the fluid phase in suspension are averaged based on volume fraction, and can be computed by

$$\rho\alpha_f = \sum_i g_i, \quad (21)$$

$$\rho\alpha_f \mathbf{u}_f = \sum_i g_i \mathbf{e}_i + \frac{1}{2} \mathbf{F}_f \Delta t. \quad (22)$$

The volume fraction and velocity of water phase can be obtained from Eqs. (21) and (22), while that of the particle phase can be calculated by Eqs. (6) and (7).

To compute the gradient terms in the color-gradient LBM and the two-fluid LBM, we employ the isotropic gradient scheme [61] with approximation to the second order as follows

$$\left. \frac{\partial \phi}{\partial x} \right|_{(x,y)} = \frac{3}{\Delta x} \sum_i [\omega_i \phi(x + e_{i,x} \Delta t, y + e_{i,y} \Delta t)] e_{i,x}, \quad (23)$$

$$\left. \frac{\partial \phi}{\partial y} \right|_{(x,y)} = \frac{3}{\Delta y} \sum_i [\omega_i \phi(x + e_{i,x} \Delta t, y + e_{i,y} \Delta t)] e_{i,y}. \quad (24)$$

At the interface between suspension and oil, water phase and particle phase is impenetrable, which is realized by another recolor operator as [60,62]

$$g_{f,i} = g_{f,i} + \beta \frac{\rho_f \rho_b}{\rho_f + \rho_b} \omega_i \frac{\nabla \rho^N}{|\nabla \rho^N|} \mathbf{c}_i. \quad (25)$$

2.4. Multiple relaxation time LBM for non-Newtonian fluid

Microgel particle suspension has been found to be a non-Newtonian fluid with wide viscosity range, which brings a huge challenge to simulations since the relaxation time range of the single-relaxation-time (SRT) LBM with BGK collision operator is very limited. To solve this problem, LBM with multiple relaxation times (MRT) has been constructed by considering the relaxation of various raw moments to their equilibria [63,64], which is adopted in this work for better accuracy and stability. It is worth mentioning that cascaded central moment LBM has been proposed and extended for multiphase flow in recent years [65,66], which yields superior stability properties compared with standard SRT and MRT approaches.

The evolution equation of MRT-LBM in matrix form is expressed as [57]

$$\mathbf{f}(\mathbf{x} + \mathbf{e}_i \Delta t, t + \Delta t) - \mathbf{f}(\mathbf{x}, t) = -\mathbf{M}^{-1} \mathbf{S} [\mathbf{m}(\mathbf{x}, t) - \mathbf{m}^{\text{eq}}(\mathbf{x}, t)] + \mathbf{M}^{-1} \left(\mathbf{I} - \frac{\mathbf{S}}{2} \right) \mathbf{G}, \quad (26)$$

where \mathbf{f} indicates the matrix form of PDF. \mathbf{M} denotes the transformation matrix, which is used to transform PDFs and discrete forces into moment space. \mathbf{S} is a diagonal matrix that contains relaxation time for each moment. \mathbf{m} , \mathbf{m}^{eq} and \mathbf{G} are the mapped moments in moment space of PDF, equilibrium PDF and discrete force, defined as $\mathbf{m} = \mathbf{M}\mathbf{f}$, $\mathbf{m}^{\text{eq}} = \mathbf{M}\mathbf{f}^{\text{eq}}$, and $\mathbf{G} = \mathbf{M}\hat{\mathbf{F}}$. Details of their mathematical expressions can be found in Appendix A.

Microgel particle suspension is a shear thinning fluid whose viscosity is related to the shear rate $\dot{\gamma}$, which can be expressed as

$$\dot{\gamma} = (2|S_{ab}S_{ab}|)^{1/2}, \quad (27)$$

$$S_{ab} = \frac{3}{2\rho\tau c^2} \sum_i f_i^{(1)} e_{ia} e_{ib}, \quad (28)$$

where the S_{ab} denotes the shear rate, the subscript a , b indicate the spatial coordinate, $f_i^{(1)}$ is first order component of Chapman-Enskog expansion and approximated by the non-equilibrium PDF as [67,68]

$$f_i^{(1)} \approx f_i^{\text{neq}} = f_i - f_i^{\text{eq}}, \quad (29)$$

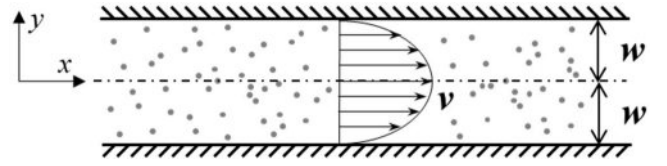


Fig. 2. Physical model of a 2D Poiseuille flow of particle suspension. The steady-state flow is driven by the pressure difference in an infinite long channel. The particles follow the fluid driven by the drag force.

2.5. Boundary conditions

The boundary conditions include solid boundaries and open boundaries. For the solid boundaries, the full-way bounce-back scheme is applied to achieve non-slip condition. For the open boundaries of fluid phase, the non-equilibrium bounce-back method proposed by Zou and He [69] is applied to achieve constant velocity or pressure conditions. For the open boundaries of particle phase, volume fraction of the fluid phase is fixed at the inlet to achieve constant particle concentration and zero-gradient Neumann boundary is applied at the outlet to achieve free outflow condition [70].

3. Numerical validations

In this section, the multiphase flow simulation method established in the previous section is to be validated by various cases, including the theoretical validations for the particle flow and suspension-oil displacement simulation, as well as comparison with experimental results. All simulations are solved on a D2Q9 lattice set.

3.1. Theoretical verifications

(1) Particle suspension flow in a microchannel

We firstly verify the LBM implementation of the classical two-fluid model (TFM) by simulating a Poiseuille flow of particle suspension. As illustrated in Fig. 2, the suspension flows in a straight channel driven by a pressure difference.

At the steady state, the TFM equations for fluid and particle phase in a straight channel are simplified into:

$$-\alpha_f \frac{\partial p}{\partial x} + \alpha_f \mu_f \frac{\partial^2 u_f}{\partial y^2} - \beta_d (u_f - u_p) = 0, \quad (30)$$

$$-\alpha_p \frac{\partial p}{\partial x} + \alpha_p \mu_p \frac{\partial^2 u_p}{\partial y^2} + \beta_d (u_f - u_p) = 0. \quad (31)$$

with a boundary condition as $u_f = u_p = 0$ at $y = -w$ or w . The analytical solution of velocity profiles of fluid and particle phases can be expressed as follow

$$\left\{ \begin{array}{l} u_i = \frac{-\partial p / \partial x}{\bar{\mu}} \left[\frac{(w+y)(w-y)}{2} - \left(1 - \frac{\bar{\mu}}{\mu_i} \right) S(y) \right] \\ S(y) = \frac{1}{\kappa^2} \left(1 - \frac{\sinh \kappa(w+y) + \sinh \kappa(w-y)}{\sinh 2\kappa w} \right) \\ \kappa = \sqrt{\beta_d \left(\frac{1}{\alpha_f \mu_f} + \frac{1}{\alpha_p \mu_p} \right)} \\ \bar{\mu} = \alpha_f \mu_f + \alpha_p \mu_p \end{array} \right. , \quad (32)$$

where $i = f, p$ indicates the fluid phase and the particles phase, $\partial p / \partial x$ denotes the pressure gradient along flow direction, μ_i and β_d are the viscosity of two phase and the drag coefficient, respectively. We conduct simulations under different viscosity ratios and drag coefficients for a comprehensive benchmark. The velocity profiles in Fig. 3 show that the

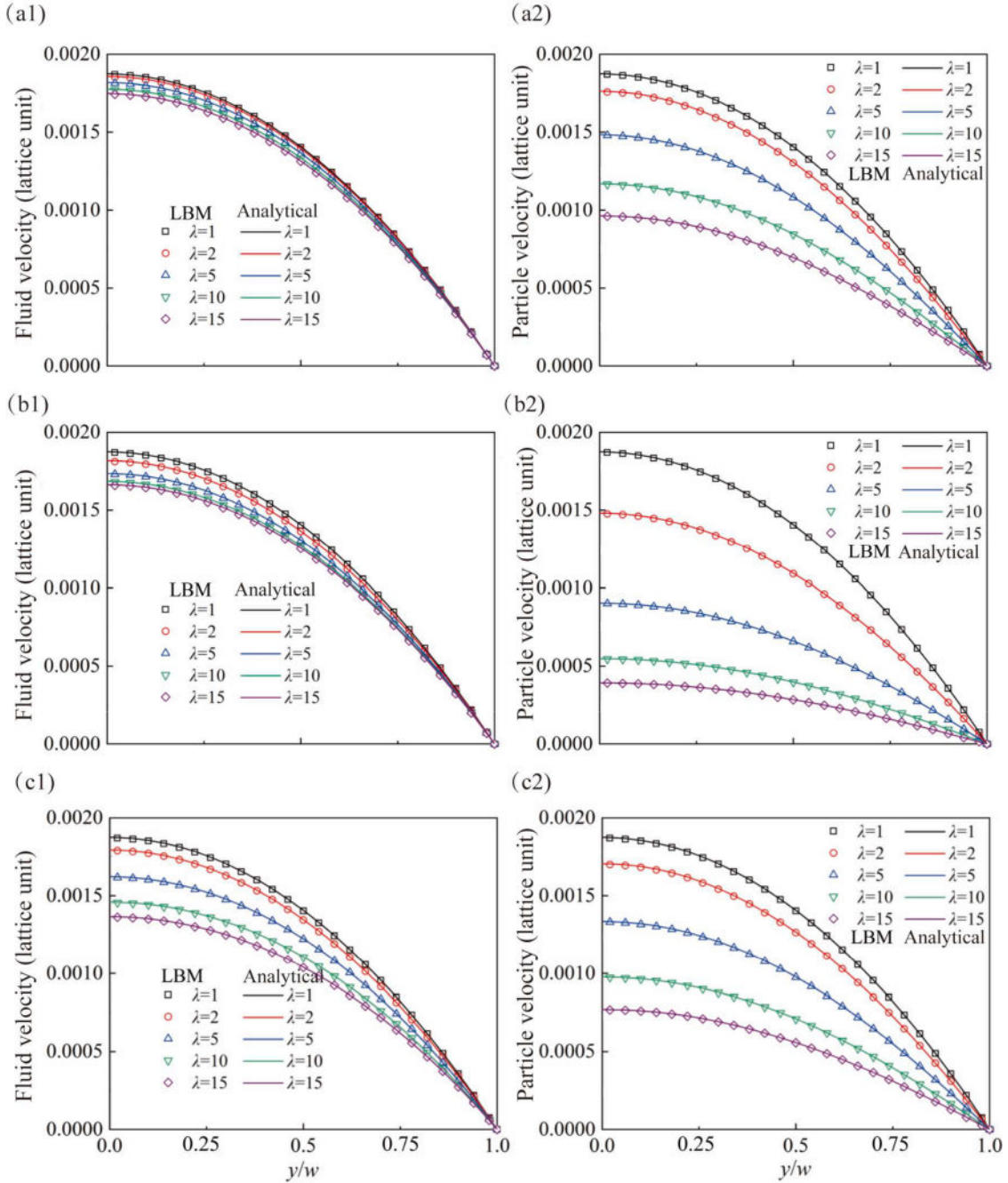


Fig. 3. Comparison of the velocity profiles for two phases in 2D particle suspension Poiseuille flow under different conditions, in which $\lambda = \mu_p / \mu_f$. The left are the results of fluid velocity profiles and the right are the results of particle velocity profile: (a) $\alpha_p = 1.0\text{vol}\%$, $\beta = 1 \times 10^{-4}$; (b) $\alpha_p = 5.0\text{vol}\%$, $\beta = 1 \times 10^{-4}$; (c) $\alpha_p = 5.0\text{vol}\%$, $\beta = 5 \times 10^{-4}$. The open markers are from simulation and the solid lines are analytical solutions. The constant pressure boundary is applied at both the inlet and outlet with $\Delta p = 1/3 \times 10^{-3}$ in lattice unit and a grid resolution of 200×50 .

simulation results agree well with the analytical solutions of Eq. (32), which indicates the correctness and accuracy of the present LBM framework for suspension flows.

We further verify the mixture-rheology two-fluid algorithm presented in this work, in which the velocity of particle phase is determined by the local mass and momentum conservation. The benchmark case based on the 2D model shown in Fig. 2 is conducted as follows: (1) the velocity profiles of fluid and particle phase is solved by classical TFM, and then the suspension velocity can be obtained by the local conservation, (2) the apparent viscosity of suspension can be determined based on the relationship between the flow rate and the pressure gradient, and then applied to the present TFM under the same conditions, (3) the

velocity of particle phase can be obtained by local momentum conservation from present TFM and compared with that of classical TFM obtained in the first step. The results under different viscosity ratios and particle sizes are shown in Fig. 4, which demonstrate the modified TFM can capture the particle velocity well with parameters in a wide range.

Besides, the microgel particle suspension is a shear-thinning non-Newtonian fluid, which means the relationship between the dynamic viscosity and the shear rate may be expressed by a power law function as

$$\mu = K \cdot \dot{\gamma}^{n-1} \quad (33)$$

where μ , $\dot{\gamma}$, K , n indicate the viscosity, the shear rate, the flow consistency index and the flow behavior index, respectively. Here, we present a

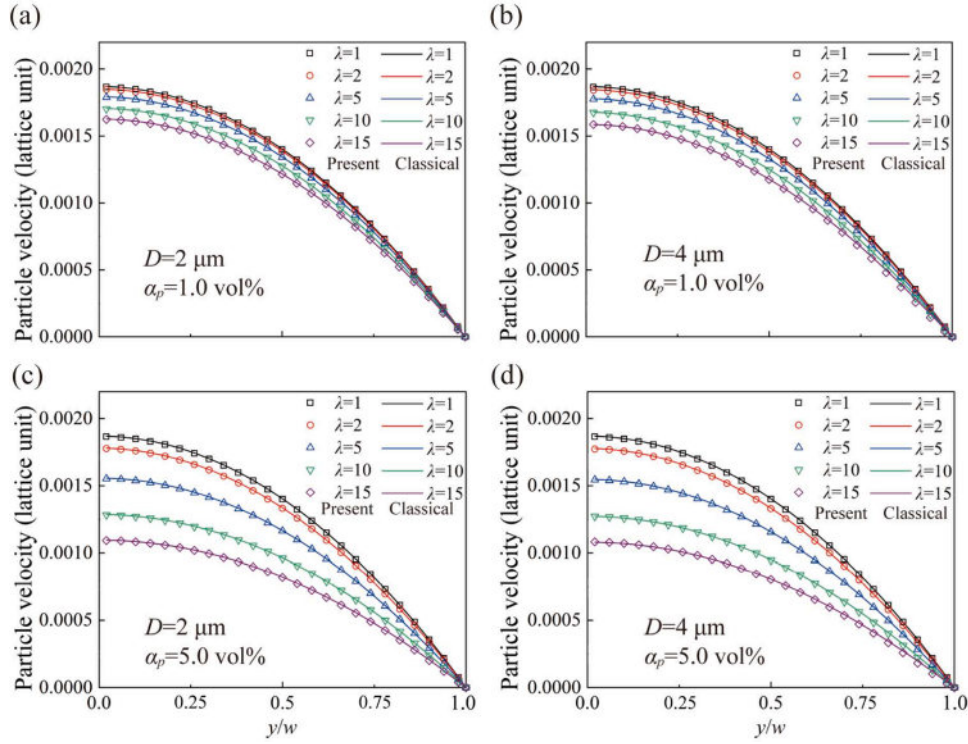


Fig. 4. Comparison of particle phase velocity profiles from classical TFM model (solid line) and present model (hollow symbol) with varying viscosity ratio $\lambda = \mu_p / \mu_f$, particle size D and particle volume fraction α_p : (a) $D = 2 \mu\text{m}$, $\alpha_p = 1.0 \text{ vol}\%$, (b) $D = 4 \mu\text{m}$, $\alpha_p = 1.0 \text{ vol}\%$, (c) $D = 2 \mu\text{m}$, $\alpha_p = 5.0 \text{ vol}\%$, (d) $D = 4 \mu\text{m}$, $\alpha_p = 5.0 \text{ vol}\%$. The boundary condition and grid resolution are the same as in Fig. 3.

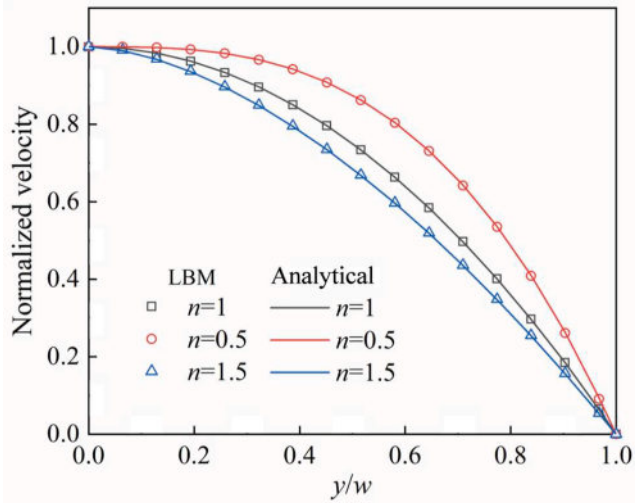


Fig. 5. Velocity profiles of power law fluid flowing in 2D channel with different values of flow behavior index. $n = 1$ represents Newtonian fluid, whereas $n > 1$ and $n < 1$ indicate shear-thickening and shear-thinning behaviors, respectively. The constant pressure boundary is applied at both the inlet and outlet with $\Delta p = 1/3 \times 10^{-3}$ in lattice unit and a grid resolution of 200×30 .

verification for a laminar power law fluid flow in a 2D channel as Fig. 2 shows, whose theoretical velocity profile under a constant pressure gradient can be calculated by

$$u = \frac{n}{n+1} \left[\frac{1}{K} \left(-\frac{\partial p}{\partial x} \right) \right]^{\frac{1}{n}} w^{\frac{n+1}{n}} \left[1 - \left(\frac{y}{w} \right)^{\frac{n+1}{n}} \right] \quad (34)$$

Fig. 5 shows the results of normalized velocity profile with different values of flow behavior index, where $n > 1$ indicates a shear-thickening

fluid, and $n < 1$ indicates a shear-thinning fluid, and $n = 1$ indicates a Newtonian fluid. The velocity profile results from MRT LBM simulations have a good agreement with the analytical results, which indicates that the present numerical simulation is able to capture the non-Newtonian rheology.

(1) Suspension-oil two-phase interactions

To test the accuracy of the immiscible two-phase simulation based on color-gradient LBM, we conduct several simulations to verify the interface separation, surface tension, contact angle and stratified flow of two phase. Firstly, the density distributions of three phases around interface is shown in Fig. 6, which shows the present model successfully achieves the separation of suspension and oil phase as well as the impenetrable condition for water and particle phase at the interface.

Surface tension is an important parameter in two-phase flow and brings the pressure difference between inside and outside the droplet, which is described by the Young-Laplace equation as

$$\Delta p = \frac{\sigma}{R}, \quad (35)$$

where σ is the dimensionless surface tension, R is the dimensionless radius of droplet. Fig. 7(a) compares the pressure difference simulated by the color-gradient LBM with the theoretical results, which demonstrates the accurate characterization of surface tension.

Contact angle is another key parameter in immiscible multiphase flow simulation reflecting the interaction of water phase, oil phase and solid phase. In the benchmark case, an oil droplet is placed on a solid wall with different contact angles. The contact angle results from simulations can be quantified by wetting length of oil phase on solid walls as shown in Fig. 7(b), which yields good agreements with the theoretical values.

To test the dynamic capability of the multiphase model under different viscosity ratios, we conduct a three-layer flow simulation, as shown in Fig. 8, where the velocity profiles obtained from simulations

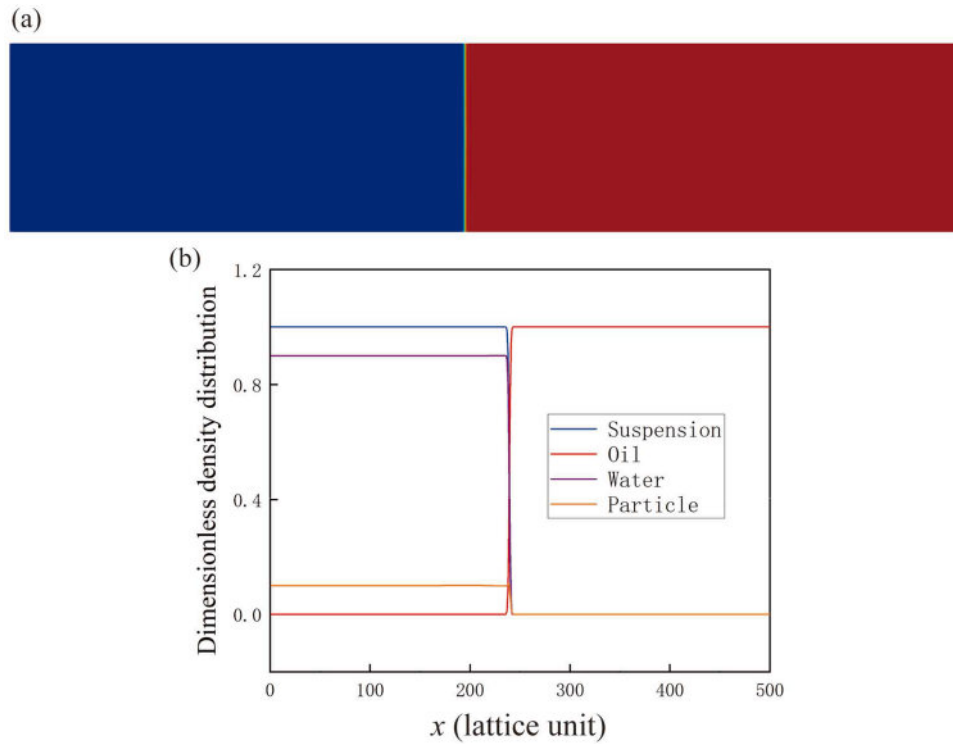


Fig. 6. Phase separation test and phase density distribution around the fluid-fluid interface. (a) Schematic of the test setup. The blue part represents the suspension phase and the red part represents the oil phase. (b) Phase density distribution around the fluid interface. The sharp change corresponds to the immiscible interface, where fluid phase separation with impenetrable condition for particle phase (yellow line) is achieved. The constant pressure boundary is applied at both the inlet and outlet with $\Delta p = 0$ in lattice unit and a grid resolution of 200×50 .

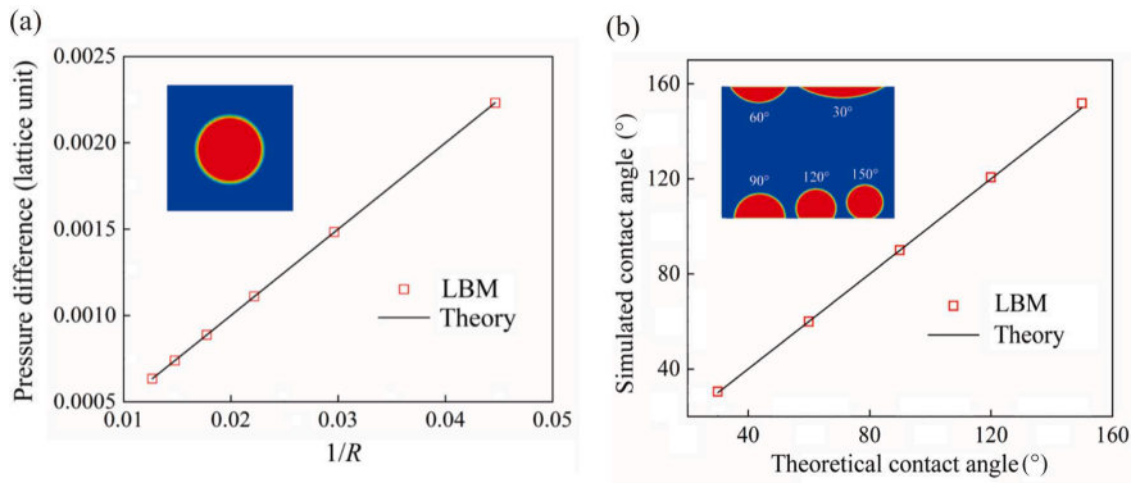


Fig. 7. Verifications of static interfaces and surface tension: (a) Young-Laplace verification, and (b) contact angle verification. The insets show typical simulation results with immiscible fluid phases. For the Young-Laplace verification, periodic conditions are applied at all open boundaries. For the contact angle verification, periodic conditions are applied at the left and right sides. The droplets stay static at the upper and lower solid walls. The grid resolutions are 200×200 .

match well with the theoretical results.

3.2. Experimental validations

In order to further validate the proposed method for realistic materials and properties, we establish an experimental platform including a microfluidic experimental module for visualization of complex flow processes and a physical property characterization module for characterization of suspension and interfacial properties. Microfluidic experiments are designed and performed to validate the capability of present

simulation method to capture the inertial effect and distribution pattern of microgel particles.

It is worth mentioning that the grid resolution should be chosen carefully for such complex fluid flow modelling under realistic conditions. The particle size in lattice unit, i.e., the ratio of characteristic particle size to grid size, should be slightly smaller than one to ensure numerical stability and model validity. If the grid resolution is too low with a small particle size in lattice unit, the drag force term (Eq. (8)) will be very large, leading to numerical instability. Moreover, liquid-liquid interfacial evolution can be inaccurate with a low grid resolution. If

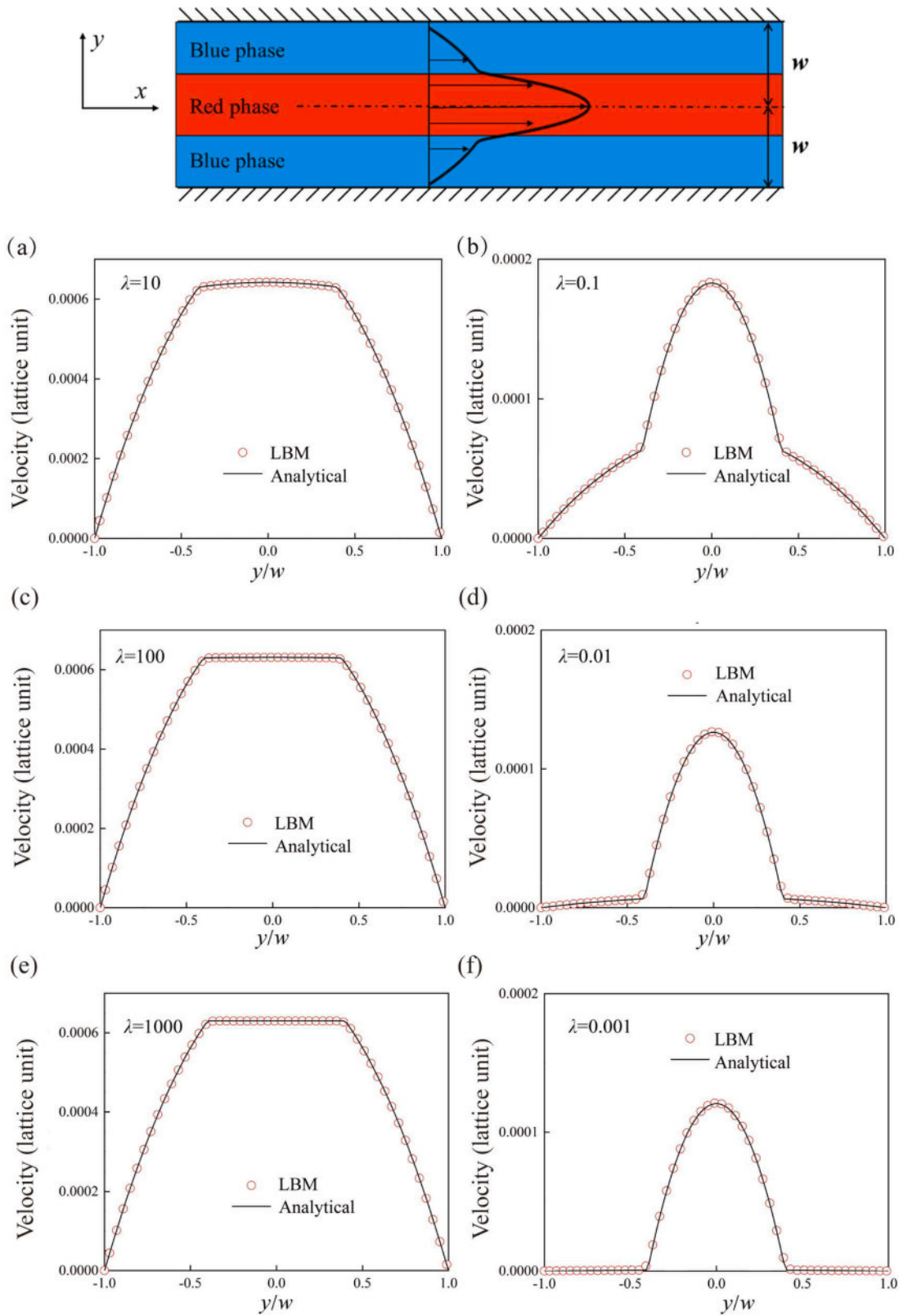


Fig. 8. Physical model of three-layer flow and velocity profiles for varying viscosity ratio $\lambda = \mu_r / \mu_b$: (a) $\lambda = 10$; (b) $\lambda = 0.1$; (c) $\lambda = 100$; (d) $\lambda = 0.01$; (e) $\lambda = 1000$; (f) $\lambda = 0.001$. The LBM results (open red circles) agree well with the analytical solutions (solid lines) under extreme viscosity ratio conditions. The body force boundary with periodic condition is applied with $F = 10^{-7}$ in lattice unit and a grid resolution of 200×100 .

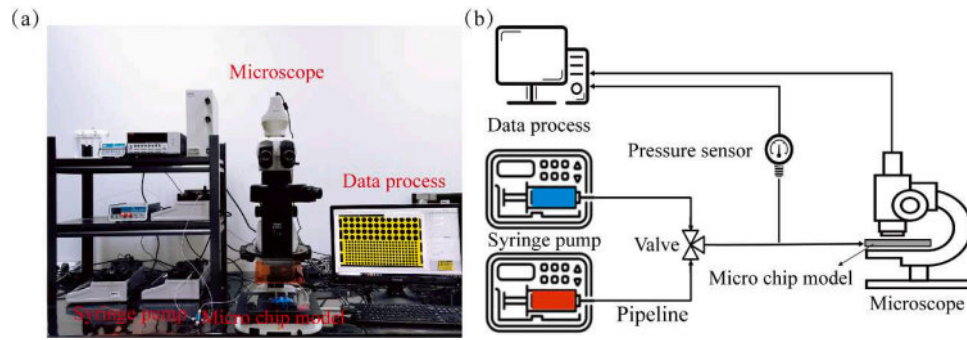


Fig. 9. Microfluidic experimental platform: (a) physical image; (b) schematic. The system mainly consists of three parts: Power source (syringe pumps), imaging (microscope, high-speed camera and microchip) and data acquisition (image processing server).

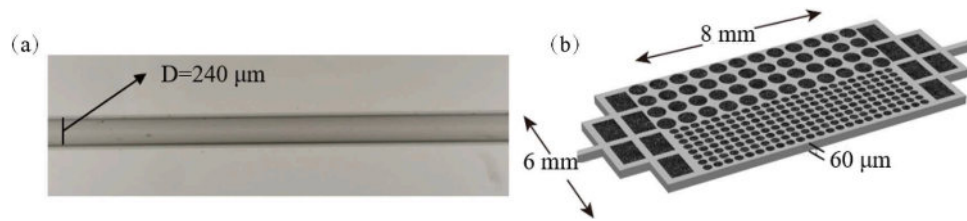


Fig. 10. Experimental models: (a) 1D capillary tube with uniform channel size (diameter 240 μm); (b) 2D chip model dual-permeability [27]. The porosity of both layers is 45% with a minimum throat size of 60 μm . The channel sizes are much larger than the characteristic particle size and plugging effects can be ignored.

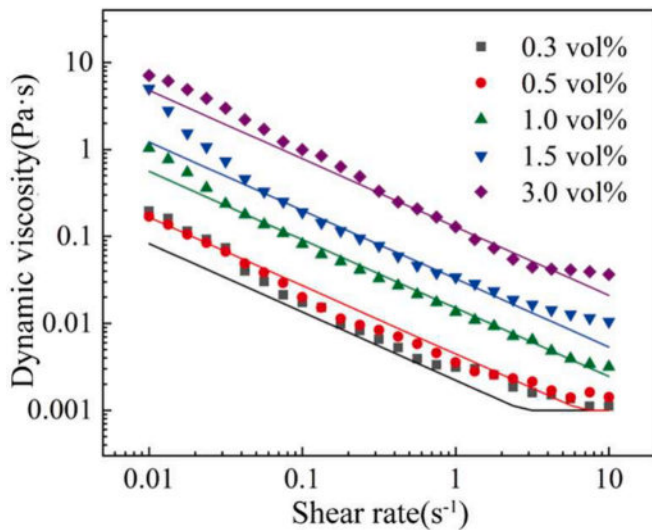


Fig. 11. Rheology property of microgel particle suspensions at different concentrations. The scatter points are experimental results and the solid lines are fitting curves applying Eq. (36). When the shear rate is higher than 10 s^{-1} , viscosity change becomes minor and a constant viscosity is applied in simulations (taken at $\dot{\gamma} = 10 \text{ s}^{-1}$). The measured mean particle diameter is $3.3 \mu\text{m}$ with a distribution ranging from 1 to $10 \mu\text{m}$. The characteristic particle size is set to be $3 \mu\text{m}$ in simulations.

the grid resolution is too high with a large particle size in lattice unit, the basic assumption of the two-fluid model will be invalid since one grid may cover less than one particle. In our simulations, the grid size is set to be twice the characteristic particle size so that the grid number at channels with minimum width is ten.

(1) Experimental platform and rheology characterization

As depicted in Fig. 9, the microfluidic experimental platform consists of a microchip, a fluorescence microscope (SMZ18, Nikon) with a high-

speed camera (DS-Ri2, Nikon), syringe pumps (Harvard Pump 11 Elite), syringes (Hamilton), and an image processing server. Fig. 10 illustrates the two types of physical models employed in this study, i.e., 1D capillary tube and 2D chip model.

Microgel particles have been found to significantly change rheology property of the aqueous phase, leading to strong interactions between particle behaviors and flow consequences [27,71]. Therefore, quantification of viscosity variations under different conditions is necessary for accurate simulation of particulate multiphase flow. We characterized the rheology of microgel particle suspensions by a rotational rheometer (Hakke Mars III, Thermo Fisher Scientific) equipped with a cone-plate geometry (C60/1° TiL) at various concentrations and shear rates. As shown in Fig. 11, microgel particle suspensions yield typical shear-thinning behavior with concentration-dependent rheology. We fit the rheology data as follows for simulation input, where the impacts of shear rate and concentration are characterized by a power law and a quadratic polynomial respectively

$$\mu = \begin{cases} (142\alpha_p^2 - 0.02\alpha_p + 0.001) \cdot \dot{\gamma}^{-0.786} & \dot{\gamma} \leq 10 \text{ s}^{-1} \\ 0.163 \cdot (142\alpha_p^2 - 0.02\alpha_p + 0.001) \dot{\gamma} & \dot{\gamma} > 10 \text{ s}^{-1} \end{cases} \quad (36)$$

(1) Particle lagging effect in a straight channel

A microfluidic experiment is designed and conducted to validate the effectiveness of the proposed simulation method in capturing inertial effect of gel particles. As shown in Fig. 12(a), a suspension slug is formed in the straight channel through injecting oil phase and suspension phase alternately. Owing to the inertial effect, the motion of microgel particles lags behind the water phase, which leads to a contrary particle distribution near the front interface and rear interface. Microgel particles accumulate at the rear interface while they are sparse near the front interface. The proposed simulation method is adopted to reproduce this process under the same condition and qualitatively consistent results with experimental observations can be obtained, as shown in Fig. 12(b). Furthermore, the quantitative distribution of particles along flow direction is obtained through image processing based on the gray distribution of experimental images. As shown in Fig. 12(c), the results from simulation and experiment are in good agreement with acceptable

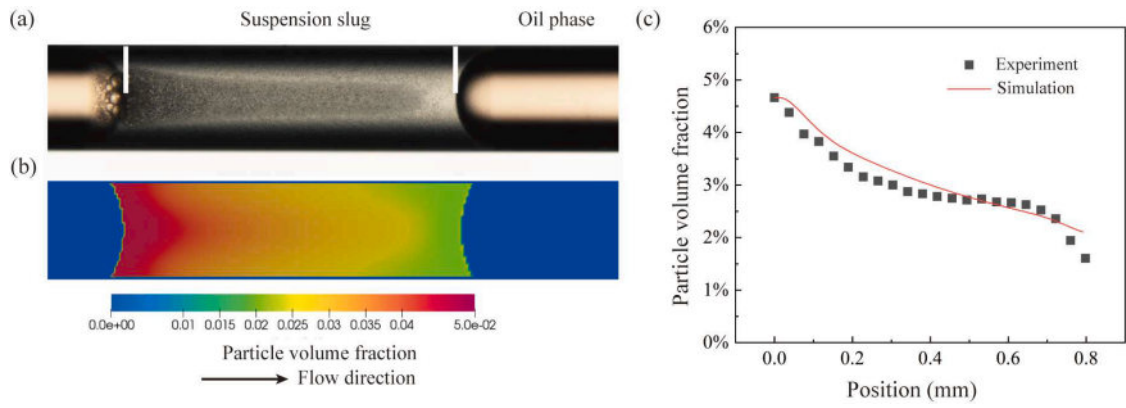


Fig. 12. Particle distribution in the suspension slug displaced by oil phase, from (a) experiment and (b) numerical simulation. The brightness in the slug in (a) represents local particle concentration, indicating a non-uniform distribution owing to particle inertial. The simulated particle distribution under 2D condition is consistent with experimental observations. (c) Concentration profile along flow direction in suspension slug. The center of the channel between the white vertical lines in (a) corresponds to position range in (c). The injected particle concentration is 3.0 vol%. The constant velocity condition with $u_{in} = 10^{-3}$ and constant pressure boundary with $p_{out} = 1/3$ in lattice unit are applied at the inlet and outlet, respectively. The grid resolution is 1000×40 .

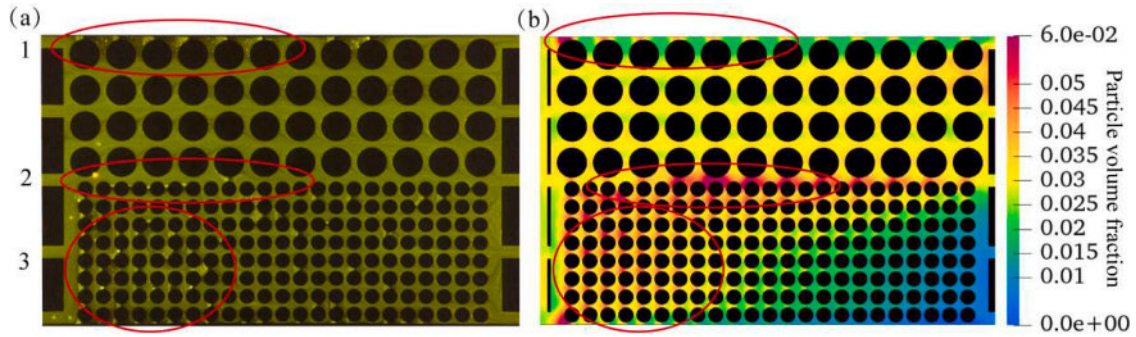


Fig. 13. Particle distribution in the dual-permeability model from (a) experiment and (b) numerical simulation. The red circles denote typical particle accumulation zones, including the edge of the high permeability zone, the inlet of the low permeability zone and the interface between two zones. The constant velocity condition with $u_{in} = 10^{-3}$ and constant pressure boundary with $p_{out} = 1/3$ in lattice unit are applied at the inlet and outlet, respectively. The grid resolution is 1620×960 .

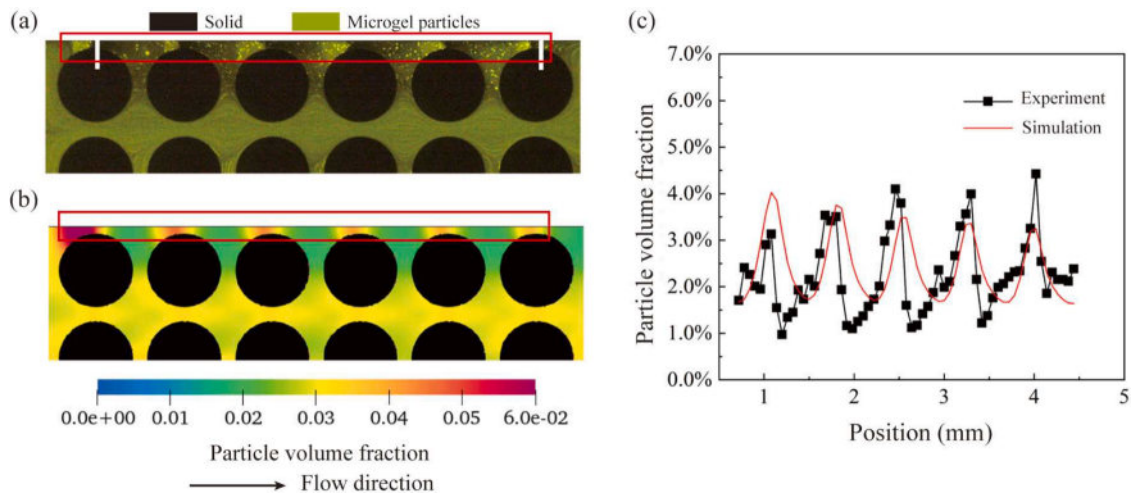


Fig. 14. Particle distribution at the top edge of the high permeability zone: (a) experimental image; (b) simulation cloud image; (c) quantitative comparison of particle volume fraction along flow direction. The green dots in (a) are retained fluorescent particles whereas streamlines reflect particles moving in a higher speed. The red squares in (a) and (b) denote typical particle accumulation zones, whereas the center of the pore space between the white vertical lines in (a) corresponds to position range in (c).

deviation, which indicates that the proposed simulation method is able to capture the lagging effect of microgel particles.

(1) Particle distribution in microfluidic porous structures

The lagging effect of particles may lead to the formation of non-uniform distribution in porous structures. To investigate this phenomenon, we conduct a microgel particle suspension flow experiment in dual-permeability model as shown in Fig. 10(b). The experimental procedure involves two steps: (1) using deionized water to displace air in microchip channels, (2) injecting microgel particle suspension with the particle concentration of 3.0 vol%. Fig. 13(a) is the fluorescence image of microgel particle distribution, which shows that microgel particles tend to accumulate at specific positions in the dual-permeability model, including the edge of the high permeability zone, the inlet of the low permeability zone and the interface between two zones. The drastic change of flow velocity at these positions results in the particle lagging and accumulation. Subsequently, a flow simulation under the same condition is conducted based on the proposed method, and the result is shown in Fig. 13(b). It can be found that our numerical simulations capture the non-uniform distribution of particles and predicts the positions of accumulation correctly.

Fig. 14(a) and (b) show the local particle distribution at the top edge of high permeability zone. It is observed that significant accumulation of particles occurs at the inlet of each throat, while only a few particles are at the outlet of each throat, forming a distinct wavy distribution along the flow direction. To quantitatively assess the accuracy of present simulation method, the volume fraction of particles at this zone is obtained from experiments based on the fluorescence intensity. These extracted values are represented by black dots in Fig. 14(c), while the results from simulation are represented by red line. The close agreement between the simulation and experimental data indicates that the present simulation method can quantitatively capture the characteristics of particle distribution.

4. Conclusions

In the present work, a numerical framework based on TFM-LBM is established to simulate the coupling transport process involving both interface evolution and microgel particle migration. Two-fluid model is successfully applied to capture the motion of amounts of particles with high efficiency by simplifying particle phase into pseudo-fluid and introducing the drag force to describe interactions between particles and the fluid phase. The mixture phase rather than the particle phase is considered in our model, which brings in several advantages including direct application of measurable apparent viscosity and easy coupling

Appendix A. Details of the MRT formulation

The transformation matrix in present work is based on Gram-Schmidt approach for D2Q9 model as follows [63]

$$M = \begin{bmatrix} 1 & 1 & 1 & 1 & 1 & 1 & 1 & 1 & 1 \\ -4 & -1 & -1 & -1 & -1 & 2 & 2 & 2 & 2 \\ 4 & -2 & -2 & -2 & -2 & 1 & 1 & 1 & 1 \\ 0 & 1 & 0 & -1 & 0 & 1 & -1 & -1 & 1 \\ 0 & -2 & 0 & 2 & 0 & 1 & -1 & -1 & 1 \\ 0 & 0 & 1 & 0 & -1 & 1 & 1 & -1 & -1 \\ 0 & 0 & -2 & 0 & 2 & 1 & 1 & -1 & -1 \\ 0 & 1 & -1 & 1 & -1 & 0 & 0 & 0 & 0 \\ 0 & 0 & 0 & 0 & 0 & 1 & -1 & 1 & -1 \end{bmatrix}. \quad (37)$$

The matrix in moment space for equilibrium PDF and discrete force are

with fluid displacement simulation. The color-gradient model is applied to capture the interface between suspension and oil. A stable and efficient simulation platform based on MRT-LBM and GPU computing is established.

A series of theoretical validations confirmed that the present method can accurately simulate particulate multiphase flow systems, including suspension flow in a microchannel, phase separation under static conditions, Young-Laplace and contact angle verifications, and three-layer flow under different viscosity ratios. Comparison with microfluidic experiments shows excellent prediction of particle lagging and non-uniform distribution in micro-channels and porous structures.

Further efforts are needed for wider applications of our model, such as capturing more complex particle behaviors, utilizing more advanced collision models and considering more realistic environmental conditions. In summary, our model provides an effective tool for studying mechanisms of microgel particles transport with significant impacts on multiphase flow in porous media.

CRedit authorship contribution statement

Qiangqiang Li: Writing – original draft, Validation, Software, Investigation. **Guang Yang:** Validation, Software. **Yunfan Huang:** Writing – original draft, Validation, Software. **Xukang Lu:** Writing – review & editing, Validation, Investigation. **Jingchun Min:** Writing – review & editing, Supervision. **Moran Wang:** Writing – review & editing, Supervision, Project administration, Conceptualization.

Declaration of competing interest

The authors declare that they have no known competing financial interests or personal relationships that could have appeared to influence the work reported in this paper.

Data availability

No data was used for the research described in the article.

Acknowledgments

This work is financially supported by the National Key Research and Development Program of China (No. 2019YFA0708704) and the NSF grant of China (No. 12272207, U1837602). We would like to sincerely acknowledge Dr. Mengquan Shi from Technical Institute of Physics and Chemistry, Chinese Academy of Sciences for his help with microgel particle synthesis.

$$m^{eq} = \begin{bmatrix} \rho \\ -2\rho + 3(u_x^2 + u_y^2) \\ \rho - 3(u_x^2 + u_y^2) \\ \rho u_x \\ -\rho u_x \\ \rho u_y \\ -\rho u_y \\ \rho(u_x^2 - u_y^2) \\ \rho u_x u_y \end{bmatrix}, \quad G = \begin{bmatrix} 0 \\ 6(u_x F_x + u_y F_y) \\ -6(u_x F_x + u_y F_y) \\ F_x \\ -F_x \\ F_y \\ -F_y \\ 2(u_x F_x - u_y F_y) \\ u_x F_y + u_y F_x \end{bmatrix}. \quad (38)$$

The relaxation matrix S for D2Q9 model is

$$S = \text{diag}[S_0, S_1, S_2, S_3, S_4, S_5, S_6, S_7, S_8], \quad (39)$$

$S_0 = S_3 = S_5 = 1$ is required to be consistent with the macroscopic equations [72]. S_7, S_8 are identical and corresponding to the kinematic viscosity, which are

$$S_7 = S_8 = \frac{1}{\tau} = \frac{2}{6\nu + 1}, \quad (40)$$

The other elements, $S_1, S_2, S_4 = S_6$, can be adjusted individually to enhance the stability and accuracy of MRT LBM algorithm [72,73].

Appendix B. Simulation framework and GPU parallel implementation

The program flowchart is shown in Fig. B.1, which simulate the coupled process of suspension-oil displacement and particle transport simultaneously with information exchanges. The particle distribution and motion required for solving particle flow are determined by the density and velocity of suspension phase, while the local viscosity under different shear rates required for solving bulk flow is determined by the volume fraction of particles.

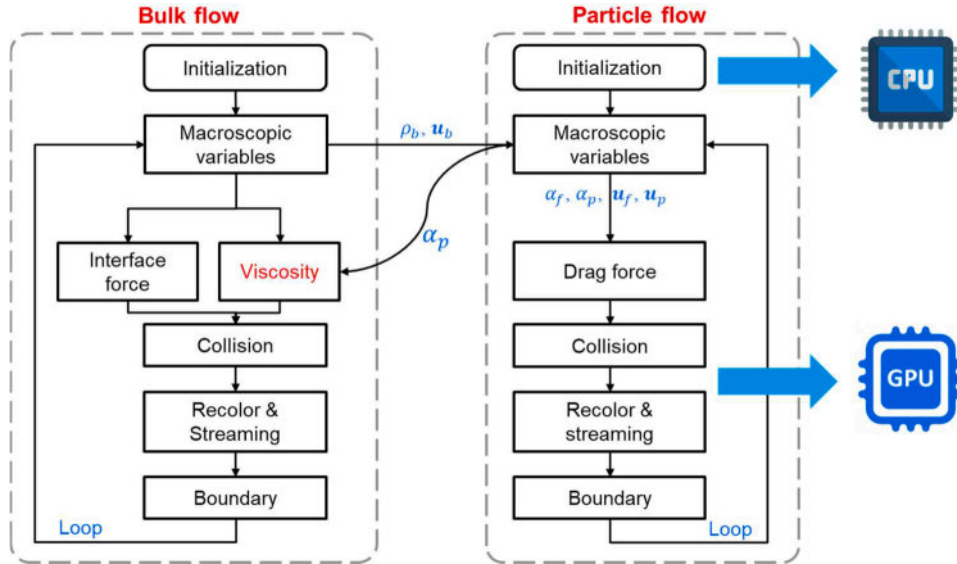


Fig. B.1. Numerical procedure of TFM-LBM with GPU computing.

The coupling simulation of three-phase system prompts large computational challenge. Therefore, GPU computing based on CUDA platform is introduced to improve the efficiency. The initialization, input and output of data are performed on CPU host while the key evolution steps, such as collision, recolor, and streaming, are computed on the GPU device. Fig. B.2 compares the computational efficiency based on CPU parallel computing and GPU computing, which shows that the GPU computing can improve computational efficiency significantly.

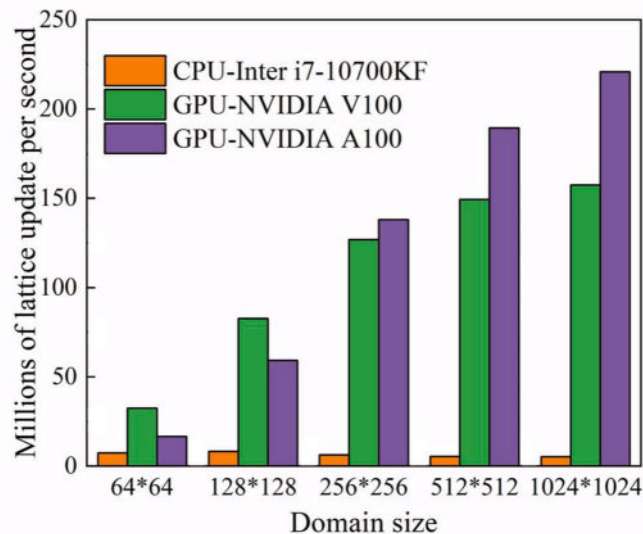


Fig. B.2. Performance comparison between GPU and CPU parallel computing.

References

- Jamaly S, Giwa A, Hasan SW. Recent improvements in oily wastewater treatment: progress, challenges, and future opportunities. *J Environ Sci* 2015;37:15–30.
- Butler JE, Snook B. Microstructural dynamics and rheology of suspensions of rigid fibers. *Annu Rev Fluid Mech* 2018;50(1):299–318.
- Lei W, Lu X, Wang M. Multiphase displacement manipulated by micro/nanoparticle suspensions in porous media via microfluidic experiments: From interface science to multiphase flow patterns. *Adv Colloid Interface Sci* 2023;311: 102826.
- More RV, Ardekani AM. Motion in stratified fluids. *Annu Rev Fluid Mech* 2023;55 (1):157–92.
- Chang HL, Sui X, Xiao L, Guo Z, Yao Y, Xiao Y, et al. Successful field pilot of in-depth colloidal dispersion gel (CDG) technology in daqing oil field. *SPE Reserv Eval Eng* 2006;9(06):664–73.
- Liu F, Wang M. Wettability effects on mobilization of ganglia during displacement. *Int J Mech Sci* 2021;106933.
- Berli CL, Quemada D. Prediction of the interaction potential of microgel particles from rheometric data. Comparison with different models. *Langmuir* 2000;16(26): 10509–14.
- Saunders BR, Vincent B. Microgel particles as model colloids: theory, properties and applications. *Adv Colloid Interface Sci* 1999;80(1):1–25.
- Zia RN. Active and passive microrheology: theory and simulation. *Annu Rev Fluid Mech* 2018;50(1):371–405.
- Leng J, Wei M, Bai B. Review of transport mechanisms and numerical simulation studies of preformed particle gel for conformance control. *J Pet Sci Eng* 2021: 109051.
- Liu Y, Hou J, Wang Q, Liu J, Guo L, Yuan F, et al. Flow of preformed particle gel through porous media: a numerical simulation study based on the size exclusion theory. *Ind Eng Chem Res* 2017;56(10):2840–50.
- Bai B, Liu Y, Coste JP, Li L. Preformed particle gel for conformance control: transport mechanism through porous media. *SPE Reserv Eval Eng* 2007;10(02): 176–84.
- Wang J, Liu H, Wang Z, Xu J, Yuan D. Numerical simulation of preformed particle gel flooding for enhancing oil recovery. *J Pet Sci Eng* 2013;112:248–57.
- Meakin P, Tartakovsky AM. Modeling and simulation of pore-scale multiphase fluid flow and reactive transport in fractured and porous media. *Rev Geophys* 2009;47(3).
- Sokolichin A, Eigenberger G, Lapin A, Lübert A. Dynamic numerical simulation of gas-liquid two-phase flows Euler/Euler versus Euler/Lagrange. *Chem Eng Sci* 1997; 52(4):611–26.
- Chou YJ, Gu SH, Shao YC. An Euler-Lagrange model for simulating fine particle suspension in liquid flows. *J Comput Phys* 2015;299:955–73.
- Ireland PJ, Desjardins O. Improving particle drag predictions in Euler-Lagrange simulations with two-way coupling. *J Comput Phys* 2017;338:405–30.
- Chen Y, Cai Q, Xia Z, Wang M, Chen S. Momentum-exchange method in lattice Boltzmann simulations of particle-fluid interactions. *Phys Rev E* 2013;88(1): 013303.
- Zhou K, Hou J, Sun Q, Guo L, Bing S, Du Q, et al. An efficient LBM-DEM simulation method for suspensions of deformable preformed particle gels. *Chem Eng Sci* 2017; 167:288–96.
- Lei W, Xie C, Wu T, Wu X, Wang M. Transport mechanism of deformable micro-gel particle through micropores with mechanical properties characterized by AFM. *Sci Rep* 2019;9(1):1453.
- Li G, Ye T, Li X. Parallel modeling of cell suspension flow in complex micro-networks with inflow/outflow boundary conditions. *J Comput Phys* 2020;401: 109031.
- Vincent S, De Motta JCB, Sarthou A, Estivaleres JL, Simonin O, Climent E. A Lagrangian VOF tensorial penalty method for the DNS of resolved particle-laden flows. *J Comput Phys* 2014;256:582–614.
- Feng Q, Cha L, Dai C, Zhao G, Wang S. Effect of particle size and concentration on the migration behavior in porous media by coupling computational fluid dynamics and discrete element method. *Powder Technol* 2020;360:704–14.
- Trofa M, D'Avino G, Maffettone PL. Numerical simulation of clogging in a microchannel with planar contraction. *Phys Fluids* 2021;33(8):083320.
- Jiang F, Liu H, Chen X, Tsuji T. A coupled LBM-DEM method for simulating the multiphase fluid-solid interaction problem. *J Comput Phys* 2022:454.
- Bian W, Chen X, Wang J. A critical comparison of two-fluid model, discrete particle method and direct numerical simulation for modeling dense gas-solid flow of rough spheres. *Chem Eng Sci* 2019;210:115233.
- Lei W, Li Q, Yang HE, Wu TJ, Wei J, Wang M. Preferential flow control in heterogeneous porous media by concentration-manipulated rheology of microgel particle suspension. *J Pet Sci Eng* 2022;212:110275.
- Gidaspow D. Multiphase flow and fluidization: continuum and kinetic theory descriptions. Academic Press; 1994.
- Liu G. Application of the two-fluid model with kinetic theory of granular flow in liquid-solid fluidized beds. *Granularity Mater Sci* 2018;2:3–23.
- Wu WT, Aubry N, Massoudi M. On the coefficients of the interaction forces in a two-phase flow of a fluid infused with particles. *Int J Non Linear Mech* 2014;59: 76–82.
- Wu WT, Yang F, Antaki JF, Aubry N, Massoudi M. Study of blood flow in several benchmark micro-channels using a two-fluid approach. *Int J Eng Sci* 2015;95: 49–59.
- He G, Ming P, Zhao Z, Abudula A, Xiao Y. A two-fluid model for two-phase flow in PEMFCs. *J Power Sources* 2007;163(2):864–73.
- Ge Y, Fan L-S. 3-D direct numerical simulation of gas-liquid and gas-liquid-solid flow systems using the level-set and immersed-boundary methods. *Adv Chem Eng* 2006;31:1–63.
- Jain D, Deen NG, Kuipers J, Antonyuk S, Heinrich S. Direct numerical simulation of particle impact on thin liquid films using a combined volume of fluid and immersed boundary method. *Chem Eng Sci* 2012;69(1):530–40.
- Li Y, Yang G, Zhang J, Fan L-S. Numerical studies of bubble formation dynamics in gas-liquid-solid fluidization at high pressures. *Powder Technol* 2001;116(2-3): 246–60.
- Jiang F, Liu H, Chen X, Tsuji T. A coupled LBM-DEM method for simulating the multiphase fluid-solid interaction problem. *J Comput Phys* 2022;454:110963.
- Chen S, Doolen GD. Lattice Boltzmann method for fluid flows. *Annu Rev Fluid Mech* 1998;30(1):329–64.
- Aidun CK, Clausen JR. Lattice-Boltzmann method for complex flows. *Annu Rev Fluid Mech* 2010;42(1):439–72.
- Sadeghi R, Gasner N, Khodaei S, Garcia J. Keshavarz-Motamed Z. Impact of mixed valvular disease on coarctation hemodynamics using patient-specific lumped parameter and Lattice Boltzmann modeling. *Int J Mech Sci* 2022;217:107038.

- [40] Wu B, Lu J, Lee H, Shu C, Wan M. An explicit immersed boundary-reconstructed thermal lattice Boltzmann flux solver for thermal–fluid–structure interaction problems. *Int J Mech Sci* 2022;235:107704.
- [41] Gunstensen AK, Rothman DH, Zaleski S, Zanetti G. Lattice Boltzmann model of immiscible fluids. *Phys Rev A* 1991;43(8):4320–7.
- [42] Shan X, Chen H. Lattice Boltzmann model for simulating flows with multiple phases and components. *Phys Rev E* 1993;47(3):1815–9.
- [43] Chen Z, Wang M, Chen S. Interfacial settling mode and tail dynamics of spherical-particle motion through immiscible fluids interfaces. *Chem Eng Sci* 2021;229:116091.
- [44] Swift MR, Orlandini E, Osborn W, Yeomans J. Lattice Boltzmann simulations of liquid-gas and binary fluid systems. *Phys Rev E* 1996;54(5):5041–52.
- [45] Liu H, Kang Q, Leonardi CR, Schmieschek S, Narváez A, Jones BD, et al. Multiphase lattice Boltzmann simulations for porous media applications: a review. *Comput Geosci* 2016;20:777–805.
- [46] Liu H, Ju Y, Wang N, Xi G, Zhang Y. Lattice Boltzmann modeling of contact angle and its hysteresis in two-phase flow with large viscosity difference. *Phys Rev E* 2015;92(3):033306.
- [47] Xie C, Lei W, Balhoff MT, Wang M, Chen S. Self-adaptive preferential flow control using displacing fluid with dispersed polymers in heterogeneous porous media. *J Fluid Mech* 2021;906:A10.
- [48] Qin F, Fei L, Zhao J, Kang Q, Derome D, Carmeliet J. Lattice Boltzmann modelling of colloidal suspensions drying in porous media accounting for local nanoparticle effects. *J Fluid Mech* 2023;963:A26.
- [49] Wang J, van der Hoef MA, Kuipers J. CFD study of the minimum bubbling velocity of Geldart A particles in gas-fluidized beds. *Chem Eng Sci* 2010;65(12):3772–85.
- [50] Wang T, Wang J. Two-fluid model based on the lattice Boltzmann equation. *Phys Rev E* 2005;71(4):045301.
- [51] Saintillan D., Rheology of active fluids, in: Davis, S. H.; Moin, P. (Eds.) *Annual Review of Fluid Mechanics*, Vol 50, 2018, pp. 563-92.
- [52] Wen CY, Yu YH. Mechanics of fluidization. In: *Proceedings of the chemical engineering progress symposium series*; 1966. p. 100–13.
- [53] Xu Z, Liu H, Valocchi AJ. Lattice Boltzmann simulation of immiscible two-phase flow with capillary valve effect in porous media. *Water Resour Res* 2017;53(5):3770–90.
- [54] Guo Z, Zheng C, Shi B. Discrete lattice effects on the forcing term in the lattice Boltzmann method. *Phys Rev E* 2002;65(4):046308.
- [55] Aidun CK, Clausen JR. Lattice-Boltzmann method for complex flows. *Annu Rev Fluid Mech* 2010;42:439–72.
- [56] Qian YH, d’Humières D, Lallemand P. Lattice BGK models for Navier-Stokes equation. *Europhys Lett* 1992;17(6):479–84.
- [57] Timm K, Kusumaatmaja H, Kuzmin A, Shardt O, Silva G, Viggen E. The lattice Boltzmann method: principles and practice. Berlin, German: Springer; 2016.
- [58] Brackbill JU, Kothe DB, Zemach C. A continuum method for modeling surface tension. *J Comput Phys* 1992;100(2):335–54.
- [59] Akai T, Bijeljic B, Blunt MJ. Wetting boundary condition for the color-gradient lattice Boltzmann method: validation with analytical and experimental data. *Adv Water Resour* 2018;116:56–66.
- [60] Latva-Kokko M, Rothman DH. Diffusion properties of gradient-based lattice Boltzmann models of immiscible fluids. *Phys Rev E* 2005;71(5):056702.
- [61] Leclaire S, Reggio M, Trépanier JY. Isotropic color gradient for simulating very high-density ratios with a two-phase flow lattice Boltzmann model. *Comput Fluids* 2011;48(1):98–112.
- [62] Riaud A, Zhao S, Wang K, Cheng Y, Luo G. Lattice-Boltzmann method for the simulation of multiphase mass transfer and reaction of dilute species. *Phys Rev E* 2014;89(5):053308.
- [63] Lallemand P, Luo LS. Theory of the lattice Boltzmann method: dispersion, dissipation, isotropy, Galilean invariance, and stability. *Phys Rev E* 2000;61(6):6546–62.
- [64] Luo LS, Liao W, Chen X, Peng Y, Zhang W. Numerics of the lattice Boltzmann method: Effects of collision models on the lattice Boltzmann simulations. *Phys Rev E* 2011;83(5):056710.
- [65] Ning Y, Premnath KN, Patil DV. Numerical study of the properties of the central moment lattice Boltzmann method. *Int J Numer Meth Fluids* 2016;82(2):59–90.
- [66] Hajabdollahi F, Premnath KN, Welch SWJ. Central moment lattice Boltzmann method using a pressure-based formulation for multiphase flows at high density ratios and including effects of surface tension and Marangoni stresses. *J Comput Phys* 2021;425:109893.
- [67] Chen S, He X, Bertola V, Wang M. Electro-osmosis of non-Newtonian fluids in porous media using lattice Poisson–Boltzmann method. *J Colloid Interface Sci* 2014;436:186–93.
- [68] Xie C, Zhang J, Bertola V, Wang M. Lattice Boltzmann modeling for multiphase viscoplastic fluid flow. *J Nonnewton Fluid Mech* 2016;234:118–28.
- [69] Zou Q, He X. On pressure and velocity boundary conditions for the lattice Boltzmann BGK model. *Phys Fluids* 1997;9(6):1591–8.
- [70] Lou Q, Guo Z, Shi B. Evaluation of outflow boundary conditions for two-phase lattice Boltzmann equation. *Phys Rev E* 2013;87(6):063301.
- [71] Lu X, Wang M. High-performance nanogel-in-oils as emulsion evolution controller for displacement enhancement in porous media. *ACS Appl Mater Interfaces* 2023;15(42):49554–66.
- [72] Yu Z, Fan LS. Multirelaxation-time interaction-potential-based lattice Boltzmann model for two-phase flow. *Phys Rev E* 2010;82(4):046708.
- [73] McCracken ME, Abraham J. Multiple-relaxation-time lattice-Boltzmann model for multiphase flow. *Phys Rev E* 2005;71(3):036701.